PHYSICS OF PLASMAS 21, 013701 (2014)

Modeling a planar sheath in dust-containing plasmas

T. H. Chung[a)]
Department of Physics, Dong-A University, Busan 604-714, South Korea

(Received 8 October 2013; accepted 17 December 2013; published online 8 January 2014)

One-dimensional fluid model is utilized to describe the sheath at a dust-containing plasma-wall boundary. The model equations are solved on the scale of the electron Debye length. The spatial distributions of electric potential and of the velocities and densities of charged species are calculated in a wide range of control parameters. The dust charge number, electric force, and ion drag force are also investigated. The impacts of Havnes parameter, the electron to ion temperature ratio, the ion collisionality, and the ionization on the spatial distributions of the plasma species and the incident fluxes of the ions to the wall (or to the probe) are investigated. With increase of Havnes parameter, the sheath thickness and the ion flux to the wall are reduced, whereas the ion drift velocity is increased. Enhanced ion thermal motion causes the ion flux to the wall to increase. An increase in ion collisionality with neutrals causes both the sheath thickness and the ion flux to the wall to decrease. With increase of the ionization rate, the sheath thickness is found to decrease and the ion flux collected by a probe increases. The localization of dust particles above the electrode is intensified by the increases in Havnes parameter, the electron to ion temperature ratio, collisionality, and ionization rate.
[http://dx.doi.org/10.1063/1.4861255]

I. INTRODUCTION

Small particles (dust) with sizes between a few nanometers and a few 10 μm are formed in planetary rings and comets, and earth space environment,[1,2] in devices for plasma-assisted material processing,[3,4] and in fusion devices[5,6] by plasma-surface interaction processes. Dust-containing plasmas have been used extensively for many applications of plasma processing. Depending on the application, particle nucleation can be both detrimental or beneficial to the process. In the semiconductor industry, particles are often considered a potential source for "killer defects" which may lead to device yield loss. On the positive side, particles with only a few nanometers in diameter often have novel properties which open up new applications.[7] Though it is not a major problem today, dust is considered a problem that could arise in future long pulse fusion devices.[6] In many plasma applications other than plasma fusion, dust is an unwanted element and attention has been drawn to find techniques for removing it. Development and improvement of dust detection and removal tools are underway.[8–10] Since various forces act on dust particles in plasmas, combination of these may be useful to remove dust particles.

Capacitively coupled rf discharges that are commonly utilized for plasma processing are a good candidate for experimenting dust behavior in the edge plasma of fusion device. The main observations of dust in glow discharges have been distinct cloud formations at the plasma-sheath boundary, near the rf powered electrode.[11–13] Fine dust particles present in a plasma acquire negative charge due to the higher mobility of electrons compared to that of the heavier ions. The negatively charged particles are well confined. They do not impact on the processed substrate since the sum of gravity, ion drag, and thermophoresis acting on them is in general well compensated by the sheath electric confinement force. Some important issues in dusty plasmas include the problem of determining the charge and density of dust particles, the sheath structure, and the spatial distribution of plasma species.[14–26] The ion flux entering the substrate is another important quantity for plasma processing and electrostatic probe diagnostics.

The problem of the plasma-sheath transition is still the subject of numerous recent investigations.[27–29] Recently, there has been a lot of interest in the study of plasma sheath in the presence of dust particles, both regarding fundamental plasma research and technological applications. In plasma processing reactors, negatively charged dust particles appear as contamination to etching, sputtering, and deposition processes. The sheath containing negatively charged dust particles is, therefore, relevant to plasma-wall interaction in various plasma-aided engineering devices including controlled fusion devices.[9] The plasma sheath provides the fluxes of ions, radicals, and dust particles to the substrate. Different features and the quality of a plasma-assisted surface processing depend strongly on the characteristics of the plasma sheath. Therefore, the study of plasma sheath with positive ions and charged dust microparticles is of great technological importance in many industrial applications of plasma processing.[14–17]

In this work, we propose a planar sheath model to characterize the behavior of dust particle. In a previous paper,[30] fluid models for collisionless plasmas with cold ions and weakly collisional plasmas with a finite ion temperature were developed for studying the structure of the plasma-planar probe boundary in low-pressure electronegative discharges. In this study, the model is extended to include the

[a)]Electronic address: thchung@dau.ac.kr

effect of dust particles for plasma-plane wall (or probe) boundary. The dust concentration, finite ion temperature, gas pressure, and the ionization frequency affect the sheath formation in dust-containing plasmas. The spatial distributions of electric potential and of the velocities and densities of charged species (ions, electrons, and dust grains) are calculated in front of a negatively biased planar wall (or probe) immersed in dust-containing plasmas. Also, the evolutions of the dust charge number, electric force, and ion drag force in a cathode sheath are calculated in a wide range of control parameters. Especially, the effects of the control parameters (Havnes parameter, ion temperature, collision, and non-neutrality parameter) on the ion flux collected by the probe are investigated.

This paper is organized as follows: In Sec. II, the electrostatic sheath model is introduced, the basic fluid equations and assumptions are given, and the numerical method is outlined. Section III describes a simplified model that provides the initial conditions on the velocities of the ions and dust grains entering the sheath. The results of the numerical simulations for the sheath structure and the density and velocity distributions of the charged species and microparticles are presented and discussed in Sec. IV. Finally, the paper is concluded in Sec. V with a summary of the main results and their brief discussion.

II. MODEL EQUATIONS

We consider the plasma of the initial number density n_0 consisting of the hot electrons (temperature T_e), and singly charged positive ions (temperature T_i). When the dust particles (density n_d, grain radius a) are immersed in the plasma they typically acquire high negative charge (up to a few thousand electrons) due to the high electron mobility and modify the equilibrium charge quasineutrality condition as[10]

$$n_i - n_e - Z_d n_d = 0, \tag{1}$$

where n_i and n_e are the ion and electron densities, and Z_d is the dust charge number. In this study, the dominant charging mechanism is assumed to be the accumulation of electrons and ions to the surface of the dust grain. Dust particles are assumed to be the spherical particles. Because the ions are heavier than the electrons, the ion current to a dust particle is smaller than the electron current, and the dust particle becomes negatively charged. In laboratory plasmas where secondary emission processes due to radiation absorption and to hot particle impacts are small, the dust particle net charge is negative.[26] The thermal electron current to the particle in the sheath is given by

$$I_e = -\pi a^2 n_e e \left(\frac{8kT_e}{\pi m_e}\right)^{1/2} \exp\left(\frac{e\phi_d}{kT_e}\right) \quad (\phi_d < 0), \tag{2}$$

$$I_e = -\pi a^2 n_e e \left(\frac{8kT_e}{\pi m_e}\right)^{1/2} \left(1 + \frac{e\phi_d}{kT_e}\right) \quad (\phi_d > 0), \tag{3}$$

where e is the electron charge, k is the Boltzmann constant, m_e is the mass of the electrons, and ϕ_d is the surface floating potential of the dust particle ($\phi_d = -Z_d e/4\pi\varepsilon_0 a$). The orbit motion limited (OML) theory can be used to calculate the charging ion currents as

$$I_i = \pi a^2 n_i e \left(\frac{8kT_i}{\pi m_i}\right)^{1/2} \left(1 - \frac{e\phi_d}{kT_i}\right) \quad (\phi_d < 0), \tag{4}$$

where m_i is the mass of the ion. For positively charged dust grains ($\phi_d > 0$), I_i has a dependence of $\exp(e\phi_d/kT_i)$ instead of $1 - e\phi_d/kT_i$.

Requiring a zero net current onto the negatively charged dust particle, Eqs. (2) and (4), and using charge neutrality condition, Eq. (1), we have

$$\sqrt{\frac{m_i T_e}{m_e T_i}}\left(1 + \frac{4\pi\varepsilon_0 a k T_e}{e^2}\frac{n_d}{n_0}\frac{e\phi_d}{kT_e}\right)\exp\left(\frac{e\phi_d}{kT_e}\right) + \frac{e\phi_d}{kT_i} - 1 = 0, \tag{5}$$

where ε_0 is the permittivity of the vacuum.

If we introduce the Havnes parameter $P = (4\pi\varepsilon_0 a k T_e/e^2)(n_d/n_0)$, Eq. (5) gives an equation for the reduced surface floating potential $\tilde{\phi}_d = Z_d e^2/4\pi\varepsilon_0 a k T_e$ as

$$\exp(\tilde{\phi}_d) = \frac{(1 - P\tilde{\phi}_d)\sqrt{\dfrac{m_i}{m_e}\gamma}}{1 + \gamma\tilde{\phi}_d}, \tag{6}$$

where γ defines the temperature ratio $\gamma = \frac{T_e}{T_i}$.

We assume that the ion density is unaffected by the presence of the dust component and thus $n_i = const = n_0$. Therefore, for a given $P_0 = (4\pi\varepsilon_0 a k T_e/e^2)(n_{d0}/n_0)$, Eq. (6) provides the dust charge (via $\tilde{\phi}_{d0}$) at the plasma bulk region. In order to obtain some physical insight in the theoretical analysis, we introduce a set of reference parameters, typical for plasma processing experiments. The plasma parameters are chosen to be $n_0 = 1.5 \times 10^{10}\,\mathrm{cm}^{-3}$, $T_e = 2\,\mathrm{eV}$, $T_i = 0.2 - 0.02\,\mathrm{eV}$, and the average particle size $a = 6\,\mu\mathrm{m}$. We fix the plasma density n_0; but keep the Havnes parameter P as a free quantity varying it in a physically meaningful range of dust densities. Taking as a maximal value, the dust number density $n_{d0} = 1.8 \times 10^6\,\mathrm{cm}^{-3}$ gives $P_{max} = 1$.

Figure 1 shows the calculated evolution of $\tilde{\phi}_{d0}$ with P_0 for different γ (= 100, 50, 10) in Ar plasmas. As n_{d0} is increased, the intergrain spacing decreases, and the average grain charge is also reduced. The evolution of $\tilde{\phi}_{d0}$ with P_0 has sensitive dependence on γ. As γ decreases, the reduced surface potential increases. This is attributable to increased ion current to the dust particle. However, as P_0 is increased (n_{d0} is increased), the dependence on γ becomes weak.

We assume the sheath region lies between $z = 0$ and the wall (the presheath is neglected) with the plasma filling the half space $z < 0$, where z is the position along the vertical axis, which is in the same direction as gravity.[24] The plasma variables are calculated along the distance from the plasma region to any arbitrary small distance near the planar wall using a set of coupled equations including the steady state fluid equations of continuity and motion for the ion, the dust particle, Poisson equation with Boltzmann electron.[31,32] The

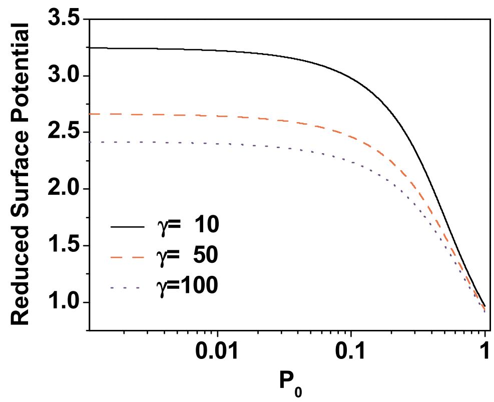

FIG. 1. Calculation of the reduced surface potential ($\tilde{\phi}_{d0}$) as a function of P_0 based on hot ion theory for different γ (= 100, 50, 30).

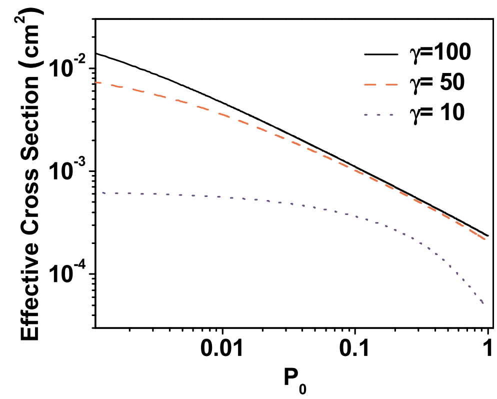

FIG. 2. Evolution of the effective scattering cross section (σ_{eff}) as a function of P_0 for different γ.

model equations are developed for a planar geometry with the assumption of one-dimensional motion of charged species towards the wall.

The ions are governed by the continuity and momentum balance equations

$$\frac{d}{dz}(n_i v_i) = \nu_{iz} n_e, \tag{7}$$

$$m_i n_i v_i \frac{dv_i}{dz} = -e n_i \frac{d\phi}{dz} - \frac{dp_i}{dz} - m_i n_e \nu_{iz} v_i - m_i n_i (\nu_{in} + \nu_{id}) v_i, \tag{8}$$

where p_i and v_i are the pressure and fluid velocity of the ions, ν_{iz} is the ionization frequency, ν_{in} and ν_{id} are the ion momentum-transfer collision frequencies with neutrals and with dust particles, and ϕ is the electric potential. The third term on the right-hand side of Eq. (8) represents the decrease of fluid momentum as ions are born at rest.[33] The fourth term represents ion drag forces due to collisions with neutrals and dust particles.[24] The ν_{in} and ν_{id} are written as[10]

$$\nu_{in} = n_n \sigma_{in} \sqrt{\frac{T_i}{m_i}}, \quad \nu_{id} = n_d \sigma_{eff} \sqrt{\frac{T_i}{m_i}}, \tag{9}$$

where n_n is the neutral number density, and σ_{in} and σ_{eff} are the momentum transfer cross section for ion-neutral collisions and for the ion-dust collisions, respectively. The effective scattering cross section in the ion-dust collisions can be written as

$$\frac{1}{\sigma_{eff}} = \frac{1}{\sigma_{id}} + \frac{4}{\pi \triangle^2}, \tag{10}$$

where $\sigma_{id} = (2\sqrt{2\pi}/3)(\tilde{\phi}_d \gamma a)^2 \Lambda$ (Λ is the modified Coulomb logarithm) is the scattering cross section for an individual grain and the second term represents a cross section corresponding to the largest admissible impact parameter $\sim\triangle/2$ ($\triangle \simeq n_{d0}^{-1/3}$ is the average interparticle distance). Figure 2 represents the evolution of σ_{eff} for dust grains with a radius of 6 μm as a function of P_0 for different γ. The σ_{eff} decreases with increasing P_0. In very diluted dust formations ($P \to 0$), the σ_{eff} mainly consist of the scattering cross section for an individual isolated grain, while in extremely dense clouds ($P \to \infty$), the $\sigma_{eff} \to \pi\triangle^2/4$.[10] As γ is decreased (i.e., T_i is increased for a fixed T_e), the cross section becomes lower due to higher thermal motion of ions. It should be noted that ν_{id} depends strongly on n_d and a (thus, P_0), and γ.

The Poisson's equation is written as

$$\varepsilon_0 \frac{d^2\phi}{dz^2} = -e(n_i - n_e) + eZ_d n_d. \tag{11}$$

We assume that electrons follow the Boltzmann energy distribution

$$n_e = n_{e0} \exp\left(\frac{e\phi}{kT_e}\right), \tag{12}$$

where n_{e0} is the electron density at the plasma bulk region.

Among the forces acting on the dust microparticles, the electric, gravitational, and ion drag are considered. The particulate trapping is clearly caused by the force balance of the electrostatic potential and the gravity, as well as the ion drag due to the ion streaming to the electrode. Therefore, the equation of motion for a dust particle is written as

$$m_d v_d \frac{dv_d}{dz} = eZ_d \frac{d\phi}{dz} + F_g + F_i, \tag{13}$$

where v_d is the velocity of the dust particle, $F_g (= 4\pi a^3 \rho_d g/3)$ is the gravitational force, and F_i is the ion drag force, which is given by[19]

$$F_i = \pi a^2 n_i m_i v_i^2 \left(1 - \frac{2e\phi_d}{m_i v_i^2}\right) + \frac{2\pi a^2 n_i (e\phi_d)^2 ln\Lambda}{m_i v_i^2}. \tag{14}$$

The charge number of a micron size dust particle (Z_d) in the sheath can be determined by the electron and ion currents striking the particle.

We assume that the dust particle flux is conserved in the sheath as

$$\frac{d}{dz}(n_d v_d) = 0. \tag{15}$$

The variation of plasma variables in the plasma-wall transition region can be characterized with several scale lengths.[29] The ionization length or the ion mean free path can be used for observing the variation of plasma variables in the sheath region. On the other hand, the electron Debye length can be used as a scale length for the sheath region since the sheath width extends only a few electron Debye length. The solution of the model equations describes the structure of the sheath region in front of a planar wall. We have the dimensionless functions and parameters

$$\xi = \frac{z}{\lambda_D}, \quad \tilde{n} = \frac{n_i}{n_{e0}}, \quad \tilde{n}_d = \frac{n_d}{n_{e0}}, \quad u = \frac{v_i}{c_s}, \quad u_d = \frac{v_d}{c_{sd}},$$
$$\eta = -\frac{e\phi}{kT_e}, \quad q = \frac{\lambda_D \nu_{iz}}{c_s}, \quad \delta_{in} = \frac{\nu_{in}}{\nu_{iz}}, \quad \delta_{id} = \frac{\nu_{id}}{\nu_{iz}}, \tag{16}$$

where c_s is the ion acoustic speed ($= \sqrt{kT_e/m_i}$), c_{sd} is the dust acoustic speed ($= \sqrt{ZkT_e/m_d}$) ($Z = P_0/(1 - P_0\tilde{\phi}_{d0})\tilde{n}_{d0}$),[23,24] and λ_D is the electron Debye length. The q, sometimes called the non-neutrality parameter, is a measure of the ionization rate.

The dimensionless equations of ion continuity and momentum balance for the ion, the dust particle, and Poisson's equation are written

$$\frac{d}{d\xi}(\tilde{n}u) = q\, e^{-\eta}, \tag{17}$$

$$\left(u - \frac{1}{\gamma u}\right)\frac{du}{d\xi} = \frac{d\eta}{d\xi} - \frac{que^{-\eta}}{\tilde{n}} - \frac{qe^{-\eta}}{\gamma \tilde{n} u} - q(\delta_{in} + \delta_{id})u, \tag{18}$$

$$u_d \frac{du_d}{d\xi} = \frac{\tilde{n}_{d0}(1 - P_0\tilde{\phi}_{d0})}{P_0}\left(-Z_d \frac{d\eta}{d\xi} + f_g + f_i\right), \tag{19}$$

$$\frac{d\tilde{n}_d}{d\xi} = -\frac{\tilde{n}_d}{u_d^2}\frac{\tilde{n}_{d0}(1 - P_0\tilde{\phi}_{d0})}{P_0}\left(-Z_d \frac{d\eta}{d\xi} + f_g + f_i\right), \tag{20}$$

$$\frac{d^2\eta}{d\xi^2} = \tilde{n} - e^{-\eta} - Z_d \tilde{n}_d, \tag{21}$$

where f is the normalized force as

$$f_g = \frac{F_g \lambda_D}{kT_e}, \quad f_i = \frac{F_i \lambda_D}{kT_e}, \tag{22}$$

and the subscript 0 denotes the quantities evaluated at the sheath edge. Integrating Eqs. (17)–(21) with the initial values at $\xi = 0$, we obtain $\tilde{n}, u, u_d, \tilde{n}_d, Z_d, f_i, \eta$ as a function of ξ. At the sheath edge, it is assumed that the potential and the electric field are approximately zero ($\eta = 0$, $d\eta/d\xi = 0$). It should be noted that the control parameters in the model equations are P_0, δ_{in}, γ, and q. The values of a, T_e, and $\tilde{n}_{d0}$ determine P_0, and Fig. 1 provides $\tilde{\phi}_{d0}$ (and Z_{d0}). From the definition of P_0 and quasi-neutrality condition, the initial values of $\tilde{n}$ and $\tilde{n}_d$ are $1/(1 - P_0\tilde{\phi}_{d0})$ and $P_0\tilde{\phi}_{d0}/(Z_{d0}(1 - P_0\tilde{\phi}_{d0}))$, respectively. By this, we can keep n_{e0} as a constant value for the cases of varying P_0. The initial values of u and u_d at the sheath edge should be chosen.

III. SIMPLE MODEL

For collisionless, continuous, and cold ions, Eqs. (17) and (18) are reduced to

$$\frac{d}{d\xi}(\tilde{n}u) = 0, \quad u\frac{du}{d\xi} = \frac{d\eta}{d\xi}. \tag{23}$$

Then, normalized ion density and velocity, by integrating Eq. (23), are

$$\tilde{n} = \left(1 + \frac{2\eta}{u_0^2}\right)^{-1/2}, \quad u = \left(u_0^2 + 2\eta\right)^{1/2}. \tag{24}$$

The charging ion current to the dust particles, Eq. (4) can be rewritten as

$$I_i = \pi a^2 n_i e v_i \left(1 - \frac{2e\phi_d}{m_i v_i^2}\right). \tag{25}$$

Combining Eqs. (2), (3), (12), (24), and (25) with the charge equilibrium, $I_e + I_i = 0$, we obtain

$$\exp(-\tilde{\phi}_d) = \frac{\sqrt{\frac{\pi m_e}{8m_i}}\, u_0\left(1 + 2\tilde{\phi}_d/(u_0^2 + 2\eta)\right)}{(1 - P\tilde{\phi}_d)}\exp(\eta). \tag{26}$$

Then, using the boundary condition, $\eta = 0$ at $\xi = 0$, we can get

$$\exp(\tilde{\phi}_{d0}) = \frac{(1 - P_0\tilde{\phi}_{d0})}{\sqrt{\frac{\pi m_e}{8m_i}}\,(u_0 + 2\tilde{\phi}_{d0}/u_0)}. \tag{27}$$

This equation provides the relation between the dust surface potential and ion Mach number u_0, as well as the relation between $\tilde{\phi}_{d0}$ and ratio of the dust particle density to the positive density at the interface, P_0.[23] Figure 3 represents the calculated evolution of $\tilde{\phi}_{d0}$ with P_0 for different u_0 (= 1.0, 1.5, 2.0) in Ar plasmas. The calculated values of $\tilde{\phi}_{d0}$ by the cold ion theory are larger than those from the hot ion theory (Fig. 1). This can be explained by the fact that for cold ions with Mach number larger than 1, the balance of electron and ion flow to the dust particle is achieved with a higher surface

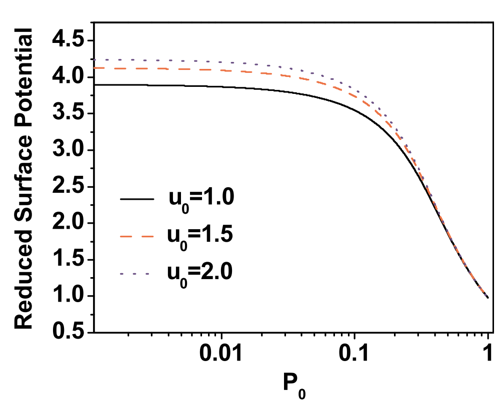

FIG. 3. Calculation of the reduced surface potential ($\tilde{\phi}_{d0}$) as a function of P_0 based on cold ion theory for different u_0 (= 1.0, 1.5, 2.0).

floating potential. As u_0 is increased, the reduced surface potential (and the average grain charge) increases, and thus, the intergrain spacing also increases. However, as P_0 is increased (n_d is increased), the dependence on u_0 becomes negligible.

If we neglect the ion drag and gravitational force, Eq. (13) (and Eq. (19)) becomes

$$u_d \frac{du_d}{d\xi} = -\tilde{\phi}_d \frac{d\eta}{d\xi}. \quad (28)$$

Integrating from $\eta = 0$ to η and setting $\Psi = -\int_0^\eta \tilde{\phi}_d \, d\eta$, we can get the dimensionless dust density utilizing Eq. (15)

$$\tilde{N}_d = \frac{n_d}{n_{d0}} = \frac{1}{\sqrt{1 + 2\Psi/u_{d0}^2}}. \quad (29)$$

Then, the Poisson's equation, Eq. (21) is written as

$$\frac{d^2\eta}{d\xi^2} = \frac{1}{1 - P_0\tilde{\phi}_{d0}}\left(1 + \frac{2\eta}{u_0^2}\right)^{-1/2} - e^{-\eta} - \frac{P_0\tilde{\phi}_d}{1 - P_0\tilde{\phi}_{d0}}\left(1 + \frac{2\Psi}{u_{d0}^2}\right)^{-1/2}. \quad (30)$$

Equation (30) can be integrated once by multiplying both sides by $d\eta/d\xi$, then we obtain

$$\frac{1}{2}\left(\frac{d\eta}{d\xi}\right)^2 + V(\eta) = \frac{1}{2}\left(\frac{d\eta}{d\xi}\right)^2_{\xi=0}, \quad (31)$$

where $(d\eta/d\xi)^2_{\xi=0} \approx 0$ is the weak presheath electric field, and Sagdeev potential is

$$V(\eta) = (1 - e^{-\eta}) + \frac{u_0^2}{1 - P_0\tilde{\phi}_{d0}}\left(1 - \sqrt{1 + 2\eta/u_0^2}\right) + \frac{P_0 u_{d0}^2}{1 - P_0\tilde{\phi}_{d0}}\left(1 - \sqrt{1 + 2\Psi/u_{d0}^2}\right). \quad (32)$$

Analogous to the analysis of a particle in the potential well, it requires the potential $V(\eta, u_0, u_{d0}) < 0$ in the sheath, which leads to

$$\left(\frac{d^2V(\eta)}{d\eta^2}\right)_{\eta=0} = -1 + \frac{1}{u_0^2(1 - P_0\tilde{\phi}_{d0})} + \frac{P_0\tilde{\phi}_{d0}^2}{u_{d0}^2(1 - P_0\tilde{\phi}_{d0})} + \frac{P_0(4\tilde{\phi}_{d0}/u_0^2 - u_0^2 - 2\tilde{\phi}_{d0})}{(u_0^2 + 2\tilde{\phi}_{d0} + 2)(1 - P_0\tilde{\phi}_{d0})} \le 0. \quad (33)$$

An analysis of a particle in the Sagdeev potential provides relations between P_0, u_0, and u_d. The ion critical Mach number $u_{0\,crit}$ depends on P_0 and u_d as well as the dust charge at $z = 0$. Figure 4(a) indicates that the ion-entering--sheath- velocity must exceed the ion sound velocity owing to the dust electrostatic drag force that is in –z direction.[23] For small P_0, the ion critical Mach number increases with P_0. The further increase of P_0 to a certain level, however, leads to a depletion of the electrons and a consequent reduction on the dust surface potential (dust charge) that makes the dust electrostatic drag force become small. Therefore, the ion critical Mach number begins to decrease. It was shown numerically by Liu *et al.*[23] that ion drift speed into the sheath reaches a maximum and decreases afterward with increasing dust density. Also, the smaller the dust Mach number is, the larger the ion critical Mach number will be. This is because that if the ion velocity relative to the dust becomes smaller, then the dust effect on the ion becomes weaker.

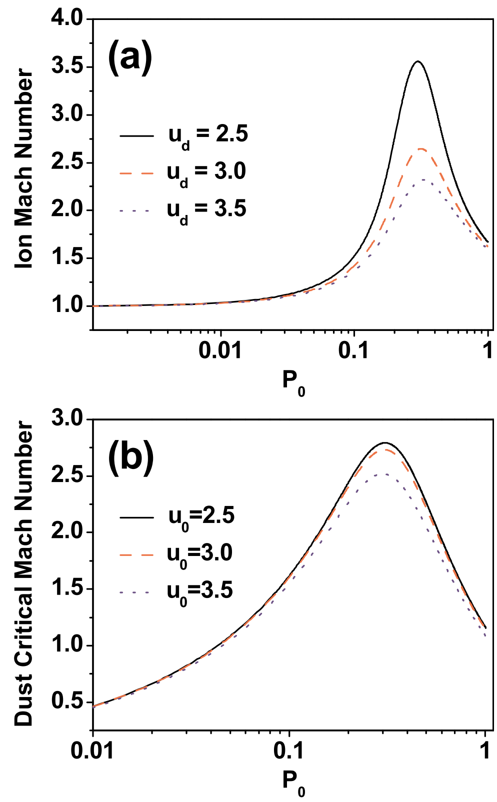

FIG. 4. (a) Ion critical Mach number versus P_0 for different dust Mach numbers u_{d0} (= 2.5, 3.0, 3.5). (b) Dust critical Mach number versus P_0 for different ion Mach numbers u_0 (= 2.5, 3.0, 3.5).

Also there exists a critical dust Mach number u_{d0} for a given condition (P_0 and u_0). The relation between the dust critical Mach number and P_0 is exhibited in Fig. 4(b). It is shown that the dust critical Mach number becomes larger first as P_0 increases, then the number begins to decline after a maximum. This is due to the fact that the ion electrostatic drag force on dust particle makes the dust entering sheath velocity larger. With the continuous increase of P_0, the dust surface potential (dust charge) is reduced, so that the dust critical number starts to decline. Also we can see, the smaller the ion Mach number is, the relatively larger the dust critical Mach number will be.

IV. RESULTS AND DISCUSSION

The main focus of this paper is placed on the investigation of the effects of Havnes parameter, the ratio of electron temperature to ion temperature, and collision and ionization rate on the spatial distributions of the electric potential, the velocities and densities of ions and electrons, the velocity and density of dust particles, the dust charge number, the electric force, and the ion drag force along the sheath toward the negatively biased planar wall.

The spatial distributions of $\tilde{n}, u, u_d, \tilde{n}_d, Z_d, f_i, \eta$ are calculated for various values of P_0, γ, δ_{in}, and q. For that purpose, Eqs. (17)–(21) are solved numerically by using the fourth-order Runge-Kutta method with the initial conditions. We have chosen the parameter; $n_0 = 1.5 \times 10^{10}\,\mathrm{cm}^{-3}$, $T_e = 2\,\mathrm{eV}$, $a = 6\,\mu\mathrm{m}$, $\rho_d = 2\,\mathrm{g/cm}^3$, $u_{d0} = 3$, and $u_0 = 1$.

Figures 5(a) and 5(b) represent the normalized electric potential and the ion velocity along the distance from the plasma ($\xi = 0$) to the wall for three different P_0 ($= 0.0001$, 0.001, 0.01). Here, $q = 0.001$, $\gamma = 100$, and $\delta_{in} = 0.2$ are used. It is seen clearly that a simple parabola is an extremely good approximation for the shape of the time averaged electric potential over the entire spatial extent of the sheath.[18] On the basis of energy conservation law (Eq. (24)), the electric potential energy of the ions in the sheath is equal to their kinetic energy, so the normalized electric potential and ion velocity distribution across the sheath are proportional to each other.[27] As P_0 is increased (for instance, as n_{d0} becomes higher for fixed n_0 and T_e), according to formula in Eqs. (9), (10), and (16), δ_{id} is increased from 0.53 ($P_0 = 0.0001$) to 2.87 ($P_0 = 0.001$) and to 9.14 ($P_0 = 0.01$). Then, with increase of P_0, the normalized electric potential and the ion velocity are found to grow rapidly (going from the plasma to the wall), and the sheath thickness becomes narrower. The rapid ion acceleration in the case of higher P_0 is related to a drastic decrease in electric potential along the sheath, which is caused by a stronger imbalance between the ion density and the negative species density in the sheath. These profiles were experimentally verified by Arnas *et al.*[25,26] The sheath modifications deduced from the observed increase in the ion velocity indicate that micron-sized particles whose charge is due to the plasma particles fluxes influence self-consistently the plasma particle distributions in their neighborhood.[26]

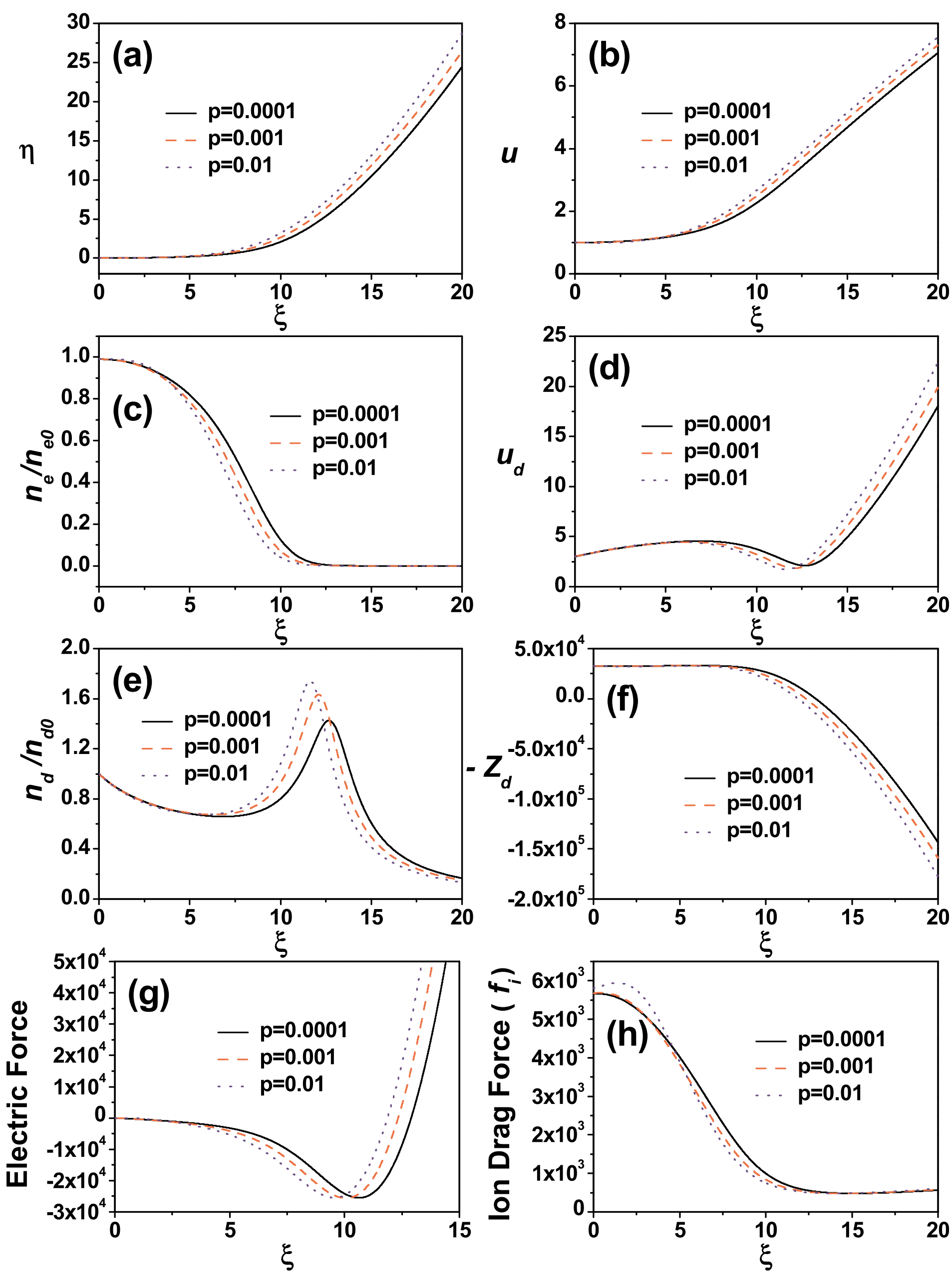

FIG. 5. (a) Normalized potential (η), (b) normalized ion velocity (u), (c) normalized electron density (n_e/n_{e0}), (d) normalized dust velocity (u_d), (e) normalized dust density (n_d/n_{d0}), (f) dust charge number ($-Z_d$), (g) electric force ($-Z_d \frac{d\eta}{d\xi}$), and (h) ion drag force (f_i) along the normalized distance for three different P_0 ($P_0 = 0.0001$, 0.001, and 0.01). Here, $q = 0.001$, $\gamma = 100$, and $\delta_{in} = 0.2$.

Figure 5(c) illustrates the normalized electron density along the distance for different P_0. It is observed that the electron density falls fast toward the wall and the sheath thickness decreases as P_0 increases. Physically speaking, as n_{d0} is increased (for fixed n_0 and T_e), more electrons attach to the dust particles, so the ion to electron density ratio rises inside the sheath.[17] Therefore, the length of non-neutral region (that is, sheath thickness) decreases with increasing P_0. A similar phenomenon can happen when T_e becomes higher for fixed n_{d0} and n_0.

In Figures 5(d)–5(f), we have examined the normalized velocity and density of the dust particles, and the dust charge number. We note that away from the sheath edge, the electric force, the gravitational force, and the ion drag force balance and the total force becomes zero. At this point, the dust velocity and its number density reach a local minimum and maximum, respectively.[15] The charge reversal point corresponds to the position of the maximum dust number density. As P_0 is increased, the charge reversal point shifts towards the sheath edge and the maximum of the trapped dust grains becomes sharp. The position of the charge reversal point is closely related to the curvature of the modeled potential, which is proportional to the electric field at the sheath edge, $E_s = kT_e/e\lambda_i$ (λ_i is the ion collision mean free path).[18] Thus, the results of the fluid theory qualitatively simulate the trapping of dust grains. To maintain a clean processing situation in plasma reactors, we should have a tool design that avoids traps and dangerous storage of dust grains during plasma process.[16] Dust grain size is a key parameter in dust management and development of dust-free surface processing in low pressure plasma tools. For a fixed condition of n_{d0}, n_0, and T_e, a decrease in the grain size results in a reduction of P_0, which leads to a less severe dust grains trap near the electrode. We note from Fig. 5(f) that the

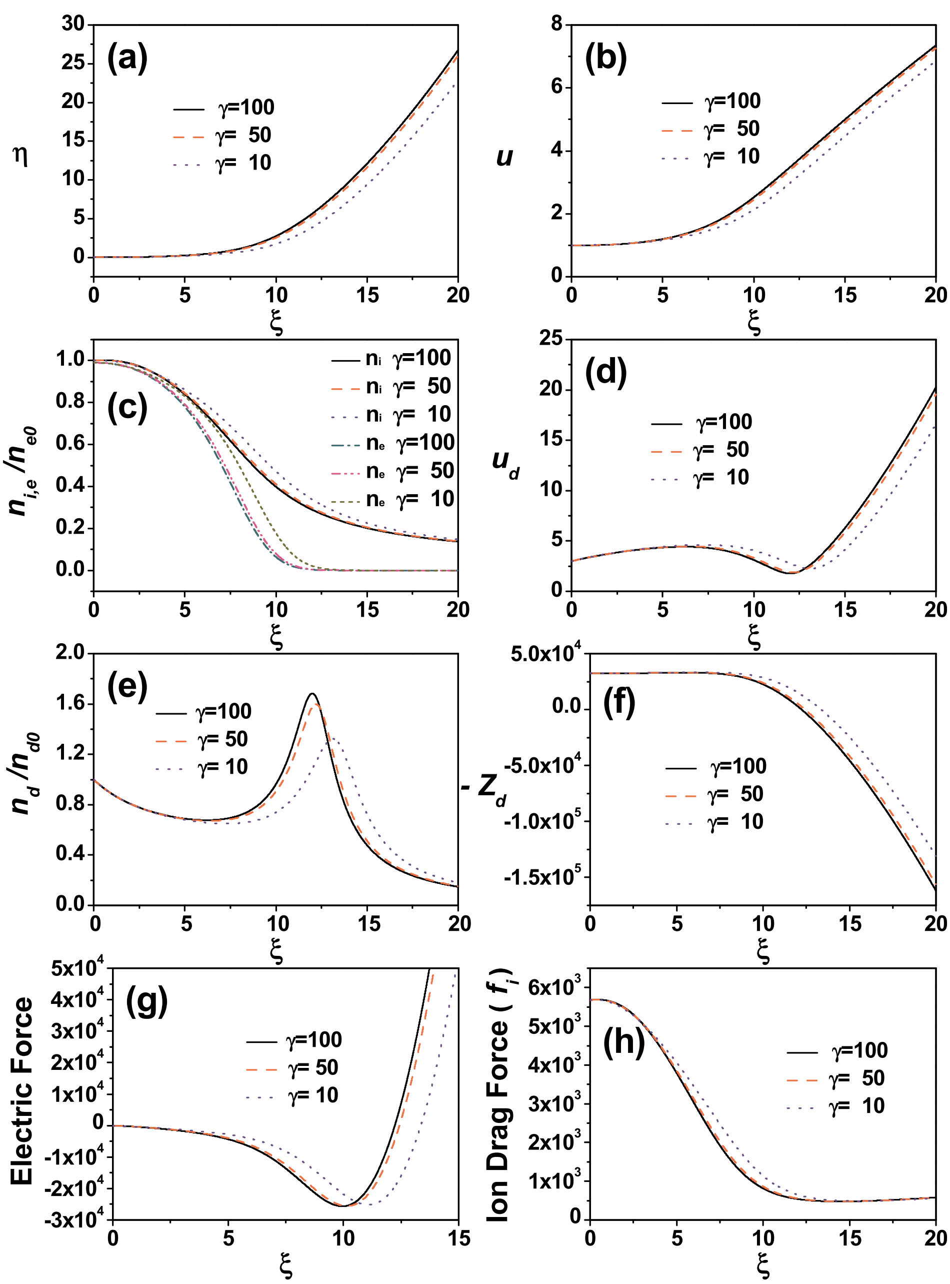

FIG. 6. (a) Normalized potential (η), (b) normalized ion velocity (u), (c) normalized densities of ions and electrons ($\tilde{n}$ and n_e/n_{e0}), (d) normalized dust velocity (u_d), (e) normalized dust density (n_d/n_{d0}), (f) dust charge number ($-Z_d$), (g) electric force ($-Z_d \frac{d\eta}{d\xi}$), and (h) ion drag force (f_i) along the normalized distance for different γ ($= 10$, 50, 100). Here, $q = 0.001$, $P_0 = 0.001$, and $\delta_{in} = 0.85$ are used.

dust charge is negative almost throughout the sheath and its absolute value decreases from the sheath edge until it changes sign abruptly somewhere close to the wall and then becomes positive. This is due to the fact that the density of electrons falls faster than that of ions in the sheath. Then, the grain charge is due only to the ion flux, where the electrons vanish and there is a pure ion sheath near the wall.[24]

The electric force and ion drag force corresponding to the three different P_0 are shown in Figs. 5(g) and 5(h). The magnitude of electric force increases with P_0 although the dust charge becomes small. As is obvious from Fig. 5(g), the electric force decelerates the dust particles along the sheath before they reach the charge reversal point and then accelerates them. On the other hand, the strength of the electric field increases with distance from the sheath edge. Therefore, the decelerating electric force increases with the distance and shows a minimum (the largest negative value) before the charge reversal point.[15] However, the ion drag force always accelerates the dust grains and its value decreases from the sheath edge due to decreased ion density, and then increases again close to the wall because of the large ion velocity. At the charge reversal point, the electric force vanishes while the ion drag force reaches a minimum. With T_e, n_0, and n_{d0} unchanged, an increase in the grain size (a) results in increased P_0. As a is increased, the ion drag force near the sheath edge increases since the ion drag force is proportional to the square of a,[16] but the ion drag force falls fast due to a drastic decrease in the ion density.

Figures 6(a) and 6(b) show the profiles of the normalized electric potential and the ion velocity for three different γ (= 10, 50, 100). Here, $q = 0.001$, $P_0 = 0.001$, and $\delta_{in} = 0.85$ are used. From the ion continuity equations, the ion density is inversely proportional to the ion velocity. So the ion density decreases towards the wall, as the ion velocity increases. As γ is increased (as T_i becomes lower for a fixed T_e), the normalized electric potential and the ion velocity increase

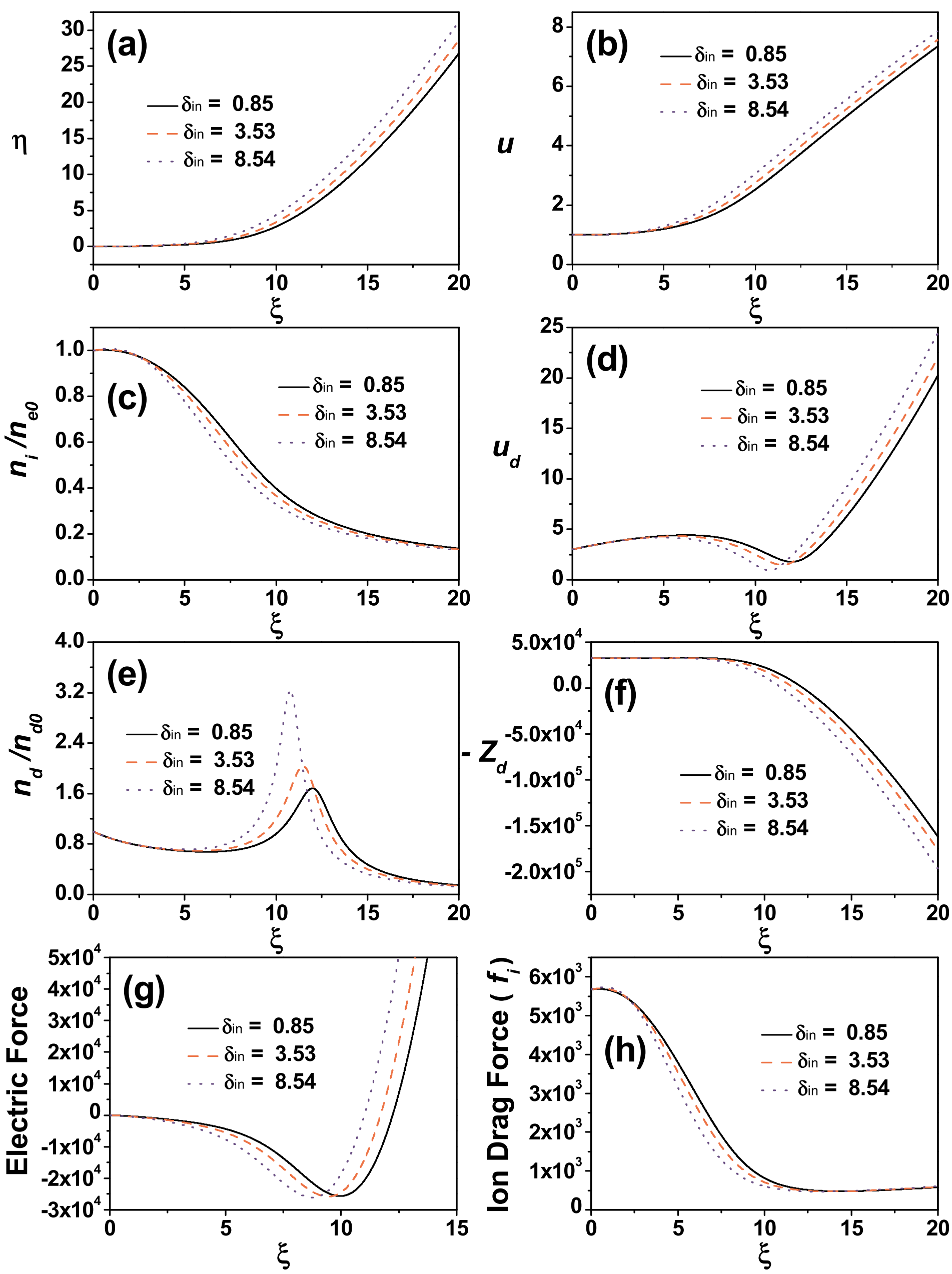

FIG. 7. (a) Normalized potential (η), (b) normalized ion velocity (u), (c) normalized ion density ($\tilde{n}$), (d) normalized dust velocity (u_d), (e) normalized dust density (n_d/n_{d0}), (f) dust charge number ($-Z_d$), (g) electric force ($-Z_d \frac{d\eta}{d\xi}$), and (h) ion drag force (f_i) along the normalized distance for three different δ ($\delta_{in} = 0.85$, 3.53, and 8.54). Here $q = 0.001$, $\gamma = 100$, and $P_0 = 0.001$.

slightly fast (going from the plasma to the wall). Figure 6(c) illustrates the profiles of the normalized densities of ions and electrons along the distance for different γ. It is observed that as γ decreases the densities of ions and electrons decrease slowly toward the wall.

Figures 6(d)–6(f) represent the spatial profiles of the normalized velocity, number density, and charge number of the dust particles. As γ is increased, the charge reversal point shifts towards the sheath edge and the maximum of the trapped dust particle density becomes sharp. In other words, enhanced ion thermal motion makes the trapped dust distribution smoothly peaked and the possibility of trapping dust particles is reduced. The electric force and ion drag force corresponding to the three different γ are shown in Figs. 6(g) and 6(h). It is observed that as γ increases the electric force becomes higher, while the ion drag force becomes lower. This can be attributed to the fact that higher γ results in higher electric field strength (higher slope of the normalized potential shown in Fig. 6(a)) and a rapid depletion of the ion density in the sheath (as shown in Fig. 6(c)).

Figures 7(a) and 7(b) represent the normalized electric potential and the ion velocity along the distance for three different δ_{in} ($= 0.85, 3.53, 8.54$). Here, $q = 0.001$, $\gamma = 100$, and $P_0 = 0.001$ are used. The δ_{in} indicates the ratio of the frequency of momentum transfer collisions with neutrals (ν_{in}) to the ionization frequency. This value defines the collisionality of ions and depends on pressure and T_i (or γ) as noted in Eq. (9). With other parameters (P_0, γ, and q) unchanged, δ_{in} can represent the pressure of plasmas. An increase in δ_{in} is found to cause the normalized electric potential and the ion velocity to increase more rapidly (going from the plasma to the wall).[34] If δ_{in} is increased for a fixed q (i.e., fixed λ_D, c_s, and ν_{iz}), the ion mean free path (λ_i) decreases, then the electric field at the sheath edge increases and the sheath thickness decreases. In a physical interpretation, an increase of collision induces the decrease of the ion flux to the wall, since the

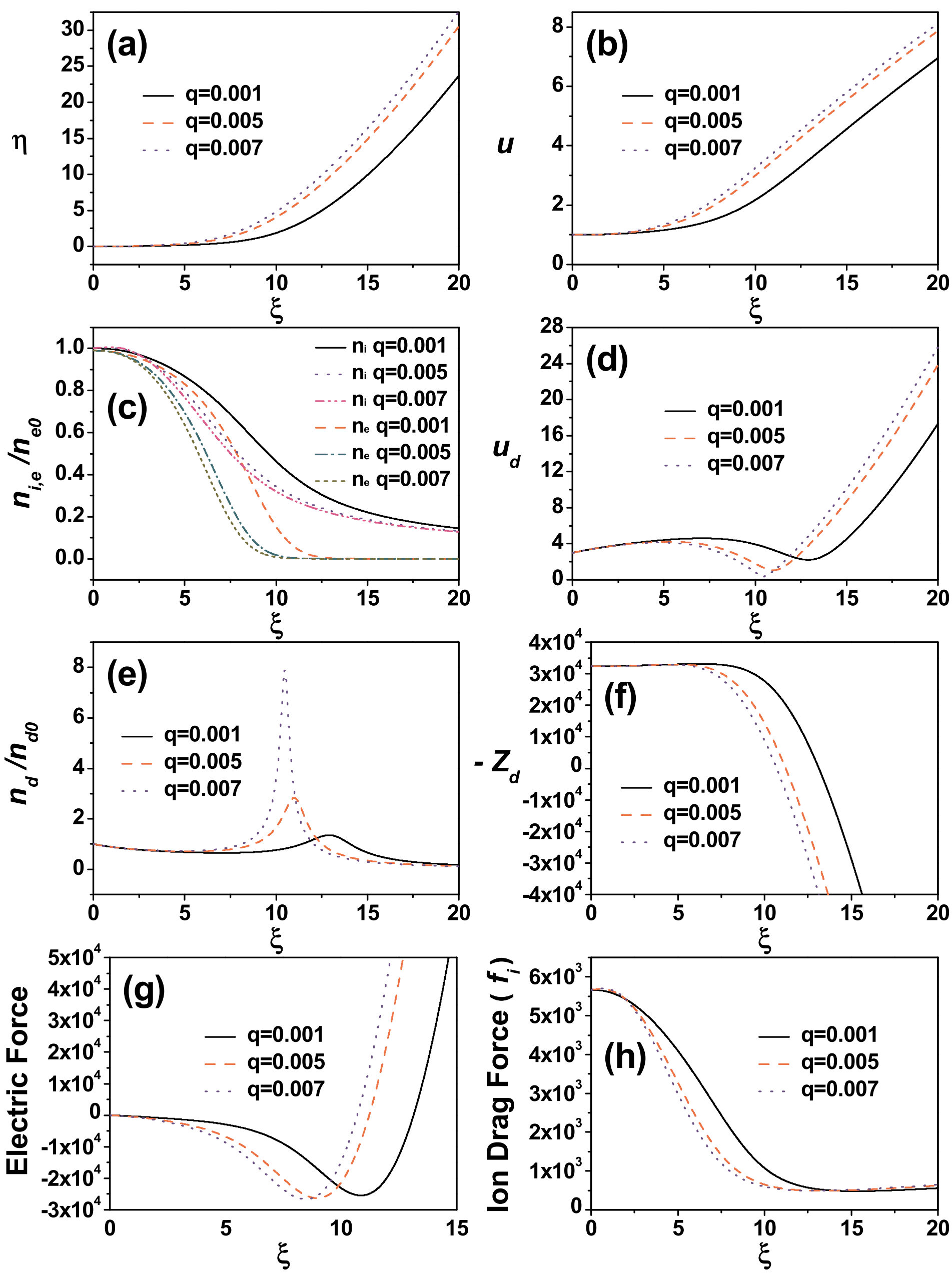

FIG. 8. (a) Normalized potential (η), (b) normalized ion velocity (u), (c) normalized densities of ions and electrons ($\tilde{n}$ and n_e/n_{e0}), (d) normalized dust velocity (u_d), (e) normalized dust density (n_d/n_{d0}), (f) dust charge number ($-Z_d$), (g) electric force ($-Z_d \frac{d\eta}{d\xi}$), and (h) ion drag force (f_i) along the normalized distance for three different q ($q = 0.001$, 0.005, and 0.007). Here, $P_0 = 0.0001$, $\gamma = 100$, and $\delta_{in} = 0.1$.

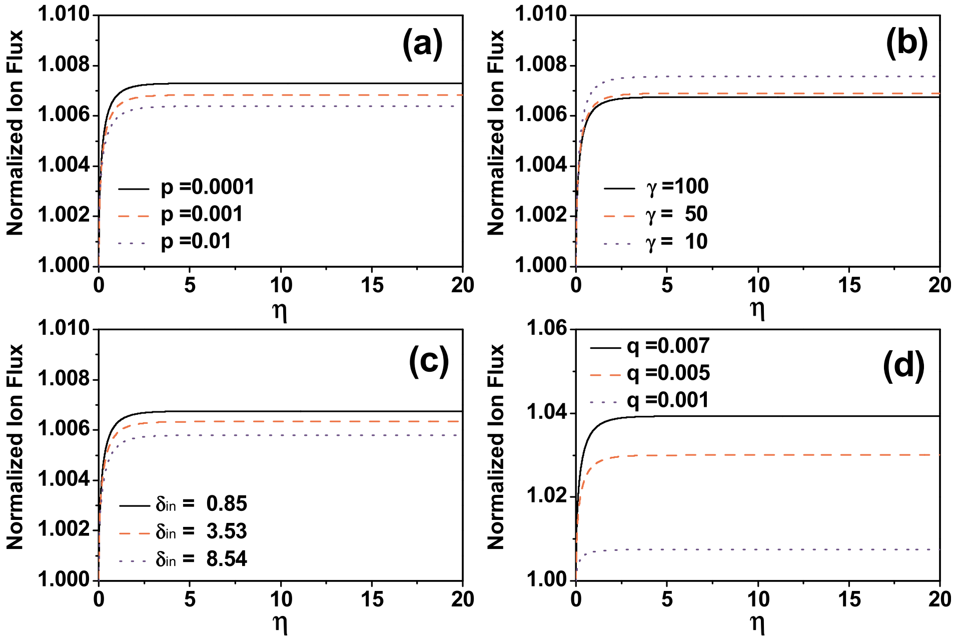

FIG. 9. Normalized ion flux entering the probe versus normalized potential for different values of (a) P_0, (b) γ, (c) δ_{in}, and (d) q.

effect produced by collisions is equivalent to a friction force.[35] It results in a decrease in the electron flux to the wall, and thus the sheath thickness decreases with increasing δ_{in}.

Figure 7(c) shows the normalized ion density along the distance for different δ_{in}. It is observed that with increasing δ_{in} the ion density falls drastically toward the wall and the sheath thickness decreases. Figures 7(d) and 7(e) are the normalized velocity and density of the dust particles. Figure 7(f) shows the dust charge number. As δ_{in} is increased, the charge reversal point shifts towards the sheath edge. Under a higher δ_{in} condition, the dust particle velocity is steeply slowed down before the charge reversal point but accelerates fast after that point, as well as it exhibits a sharp maximum in the trapped particle density. In Figs. 7(g) and 7(h), we have examined the electric force and ion drag force corresponding to the three different δ_{in}. We note that both forces decrease with increasing δ_{in}, being attributable to the drastic decrease of the ion density along the sheath.

Next, the effects of q on the sheath have been studied. The profiles of the normalized electric potential and the ion velocity at three different values of q (= 0.001, 0.005, 0.007) are indicated in Figures 8(a) and 8(b). Here, $\delta_{in} = 0.1$, $\gamma = 100$, and $P_0 = 0.0001$ are used. It is seen that as q is increased, the electric potential increases more rapidly, and the sheath thickness decreases. Also, the ion velocity becomes larger with increasing q. An increase in q under a condition with fixed P_0, γ, and δ is equivalent to either an increase in λ_D or an increase in n_n (a decrease in λ_i), thus an increase in q produces a decrease of the sheath thickness.

Figure 8(c) shows the profiles of the normalized densities of ions and electrons along the distance for different q. It is observed that the densities of ions and electrons decrease rapidly toward the wall with increasing as q, indicating a decrease in the sheath thickness. Figures 8(d)–8(f) are the profiles of the normalized velocity, density, and charge number of the dust particles, respectively. As q is increased, the dust grains are more decelerated first and accelerated fast after the charge reversal point. And the charge number changes rapidly, and the charge reversal point shifts towards the sheath edge and the maximum of the trapped dust particle density becomes sharply peaked. The electric force and ion drag force corresponding to the three different q are shown in Figs. 8(g) and 8(h). It is observed that as q is increased the electric force becomes higher, while the ion drag force becomes lower. This can be explained by the fact that higher q results in higher electric field strength (as shown in Fig. 8(a)) and a rapid depletion of the ion density in the sheath (as shown in Fig. 8(c)).

If the wall is replaced by the Langmuir probe, a point on the curve of the electric potential at the probe position, $\xi = \xi_p$, gives the normalized potential η_p. The model provides the probe characteristics of the dimensionless ion flux (current)—normalized voltage by plotting $\tilde{n}_{\xi_p} u_{\xi_p}$ versus the dimensionless electric potential η_p. Figures 9(a)–9(d) are theoretical $I - V$ curves plotted in this way. Here, we have examined the dependence of the ion flux on P_0, q, δ_{in}, and γ. It is clearly seen that the ion flux increases with q, but decreases with P_0, γ, and δ_{in}. When P_0 becomes larger, the ion flux to the probe decreases. The P_0 dependence is attributable to the increased ion collisions with dust grains. As the ions have larger thermal motion, the ion flux collected by the probe increases.[36] Figure 9(c) indicates that as δ_{in} is increased, the ion flux to the probe decreases even though the sheath thickness decreases. From Fig. 9(d), it is seen that an increase of q induces the increase of the ion flux collected by the probe because of a larger production of ions by ionization.

V. CONCLUSION

One-dimensional fluid simulations are used to describe a sheath in dust-containing plasmas. The spatial distributions of electric potential and of the velocities and densities of plasma species are calculated in front of a negatively biased planar wall. The control parameters are the Havnes parameter (P_0), the electron to ion temperature ratio (γ), the ratio of the rate coefficient for the ion momentum transfer collision to that for the ionization (δ_{in}), and the non-neutrality parameter (q). The behavior of the dust charge number, the electric force, the ion drag force, and the ion flux collected by the wall are also investigated as functions of control parameters. We have found that an increase of P_0 induces the decrease of the sheath thickness as well as of the ion flux to the wall, and that with increase of P_0, the ion drift velocity increased, and the localization of trapped dust particles is intensified. We have shown that enhanced ion thermal motion causes the ion flux to the wall to increase, and the trapped dust distribution to be less sharply peaked. With increase of the ion collision with neutrals, both the sheath thickness and the ion flux to the wall decrease, and the trapped dust distribution becomes sharply peaked. An increase of ionization causes the sheath thickness to decrease and the ion flux collected by a probe to increase, and the trapped dust distribution sharply peaked. Our results are of direct interest to the control and probe diagnostics of dust grains in various dust-containing plasmas.

ACKNOWLEDGMENTS

Helpful discussions with Professor K. S. Chung of Hanyang University and Dr. S. H. Hong of National Fusion Research Institute of Korea are greatly acknowledged. This work was supported by the National Research Foundation of Korea (NRF) funded by the Ministry of Education, Science and Technology (Grant No 20100020085, Fusion Core Research Center Program).

[1] C. K. Goertz, Rev. Geophys. **27**, 271, doi:10.1029/RG027i002p00271 (1989).
[2] O. Havnes, U. de Angelis, R. Bingham, C. K. Goertz, G. E. Morfill, and V. Tsytovich, J. Atmos. Terr. Phys. **52**, 637 (1990).
[3] G. S. Selwyn, J. Singh, and R. S. Bennett, J. Vac. Sources Technol. A **7**, 2758 (1989).
[4] L. Boufendi and A. Bouchoule, Plasma Sources Sci. Technol. **11**, A211 (2002).
[5] G. Federici *et al.*, Nucl. Fusion **41**, 1967 (2001).
[6] J. Winter, Plasma Phys. Controlled Fusion **46**, B583 (2004).
[7] Z. Shen and U. Kortshagen, J. Vac. Sources Technol. A **20**, 153 (2002).
[8] A. Barkan, N. D'Angelo, and R. L. Merlino, Phys. Rev. Lett. **73**, 3093 (1994).
[9] N. C. Adhikary, H. Bailung, A. R. Pal, J. Chutia, and Y. Nakamura, Phys. Plasmas **14**, 103705 (2007).
[10] V. V. Yaroshenko, S. A. Khrapak, and G. E. Morfill, Phys. Plasmas **20**, 043703 (2013).
[11] A. Bouchoule and L. Boufendi, Plasma Sources Sci. Technol. **2**, 204 (1993).
[12] A. Bouchoule and L. Boufendi, Plasma Sources Sci. Technol. **3**, 292 (1994).
[13] T. Nitter, Plasma Sources Sci. Technol. **5**, 93 (1996).
[14] J.-X. Ma and M. Y. Yu, Plasmas **2**, 1343 (1995).
[15] G. Foroutan, Phys. Plasmas **17**, 123711 (2010).
[16] G. Foroutan and A. Akhoundi, J. Appl. Phys. **112**, 073301 (2012).
[17] G. Foroutan and A. Akhoundi, Phys. Plasmas **19**, 103505 (2012).
[18] E. B. Tomme, B. M. Annaratone, and J. E. Allen, Plasma Sources Sci. Technol. **9**, 87 (2000).
[19] D. Wang and X. Wang, J. Appl. Phys. **89**, 3602 (2001).
[20] Y. N. Nejoh, Phys. Plasmas **8**, 3545 (2001).
[21] M. K. Mahanta and K. S. Goswami, Phys. Plasmas **8**, 665 (2001).
[22] V. N. Tsytovich, S. V. Vladimirov, and S. Benkadda, Phys. Plasmas **6**, 2972 (1999).
[23] J.-Y. Liu, Z.-X. Wang, X. Wang, Q. Zhang, X. Zou, and Y. Zhang, Phys. Plasmas **10**, 3507 (2003).
[24] D. Benlemdjaldi, A. Tahraoui, R. Hugon, and J. Bougdira, Phys. Plasmas **20**, 043508 (2013).
[25] C. Arnas, M. Mikikian, and F. Doveil, Phys. Scr. **T89**, 163 (2001).
[26] C. Arnas, M. Mikikian, G. Bachet, and F. Doveil, Phys. Plasmas **7**, 4418 (2000).
[27] A. K. Shaw, S. Kar, and K. S. Goswami, Phys. Plasmas **19**, 102108 (2012).
[28] K. U. Riemann, J. Seebacher, D. D. Tskhakaya Sr., and S. Kuhn, Plasma Phys. Controlled Fusion **47**, 1949 (2005).
[29] K. U. Riemann, IEEE Trans. Plasma Sci. **23**, 709 (1995).
[30] T. H. Chung, Phys. Plasmas **16**, 063503 (2009).
[31] R. N. Franklin, Plasma Sources Sci. Technol. **9**, 191 (2000).
[32] T. E. Sheridan, P. Chabert, and R. W. Boswell, Plasma Sources Sci. Technol. **8**, 457 (1999).
[33] T. E. Sheridan, J. Phys. D: Appl. Phys. **32**, 1761 (1999).
[34] Z. Sternovsky, Plasma Sources Sci. Technol. **14**, 32 (2005).
[35] J. I. Fernandez Palop, J. Ballesteros, M. A. Hernandez, and R. Morales Crespo, Plasma Sources Sci. Technol. **16**, S76 (2007).
[36] J. I. Fernandez Palop, J. Ballesteros, M. A. Hernandez, R. Morales Crespo, and S. Borrego del Pino, J. Appl. Phys. **95**, 4585 (2004).